Title: Experience replay facilitates the formation of the hexagonal pattern of grid cells

Bo Zhang[1,2], Lei Ma[1,3], and Jia Liu[2*]

[1] Beijing Academy of Artificial Intelligence, Beijing, 100084, China

[2] Tsinghua Laboratory of Brain and Intelligence & Department of Psychology, Tsinghua University, Beijing, 100084, China

[3] National Biomedical Imaging Center, College of Future Technology, Peking University, Beijing, 100871, China

*Correspondence shall be addressed to: JL, liujiathu@tsinghua.edu.cn

Abstract

Reverse neuronal replay, characterized by the sequential reactivation of hippocampal place cells that represents past experiences, is proposed to organize learned knowledges into a cognitive map. Here we utilized the continuous attractor model to simulate the formation of the hexagonal pattern of entorhinal grid cells, the metric for cognitive map, during the experience replay of hippocampal place cell. We found a significant enhancement in grid periodicity with reverse replay compared to that without replay. This facilitation effect was exclusive to reverse replay, as neither forward nor shuffled-experience replay elicited a similar effect. Further investigation revealed that the relationship between experience replay and hexagonal pattern formation was modulated by the interaction between the spatial scales of grid cells and the length of replayed experience, as reverse replay with lengths of past experience adapted to the scale was particularly effective in maintaining the stability of receptive fields in smaller scale grid cells. In summary, our results illustrate a causative link between experience replay and hexagonal pattern formation from a computational perspective, providing insights into how reverse reactivations of hippocampal place cells may facilitate the construction of abstract knowledge structures through the formation of the hexagonal pattern of entorhinal grid cells.

Keywords: neuronal replay, grid cell, Hippocampus, Entorhinal Cortex, continuous attractor model

Introduction

Episodic memory, closely associated with the hippocampus (HPC; Tulving and Markowitsch, 1998; Burgess et al., 2002), is metaphorically characterized as mental travel on a cognitive map (Tolman, 1948; Moser et al., 2017). This travel is guided by neuronal replay in the hippocampus for recollection of the past and anticipation of the future (Schacter et al., 2007). The structure of these episodes, fundamental to mental travels (Hafting et al., 2005; McNaughton et al., 2006; Behrens et al., 2018), is mapped by the metric provided by entorhinal grid cells, where each episode on the cognitive map is presumably represented by the positional coding of grid cells across multiple scales (Bush et al., 2015). However, the mechanism through which hippocampal neuronal replay and entorhinal grid metric work together to enable episodic memory remains unclear.

Recent studies suggest an interplay between neuronal replay and the cognitive map, wherein the former helps organize abstract knowledge derived from environmental topology to construct the latter. For example, reversed reactivation of neurons represents unique object sequence structures (Wu and Foster, 2014; Liu et al., 2019), and impaired replay, as reported in humans (Nour et al., 2021) and rodents (Suh et al., 2013) with schizophrenia, leads to deficits in structured mental representations. In line with this finding, the hexagonal pattern of entorhinal grid cells is gradually formed when rodents navigate novel environments (Barry et al., 2012), while replays are observable immediately following the first exploratory lap on novel tracks (Foster & Wilson 2006). The concurrent emergence of hexagonal patterns of entorhinal grid cells and neuronal replay of hippocampal place cells prompts a hypothesis that replay may play a pivotal role in forming the hexagonal pattern, which in turn helps construct the cognitive map.

Here, we investigated the mechanism underlying the interplay between experience replay and hexagonal pattern formation (Fig.1). To establish a causative relationship based on empirical cooccurrence, replay needs to be selectively manipulated (e.g., by intentionally turning it on and off) to assess its impact on hexagonal pattern formation, an endeavor that proves challenging in empirical studies. Therefore, we adopted a computational model to illustrate the role of replay on hexagonal pattern formation. Specifically, we utilized the continuous attractor network (CAN), also known as the spin-glass model (Fuhs and Touretzky, 2006), which is commonly used to simulate the hexagonal pattern of grid cells (Burak and Fiete, 2009; Couey et al., 2013; Shipston-Sharman et al., 2016; Kang and Balasubramanian, 2019; Khona & Fiete, 2022). In our experiment,

we designated a virtual gorilla to mimic an animal navigating novel environments (Fig.1d). We found significant enhancement in spatial periodicity in the firing pattern of grid cells after applying reverse replay, particularly effective for smaller grid scales, suggesting a role of experience replay in constructing high-resolution cognitive maps (Schuck and Niv, 2019).

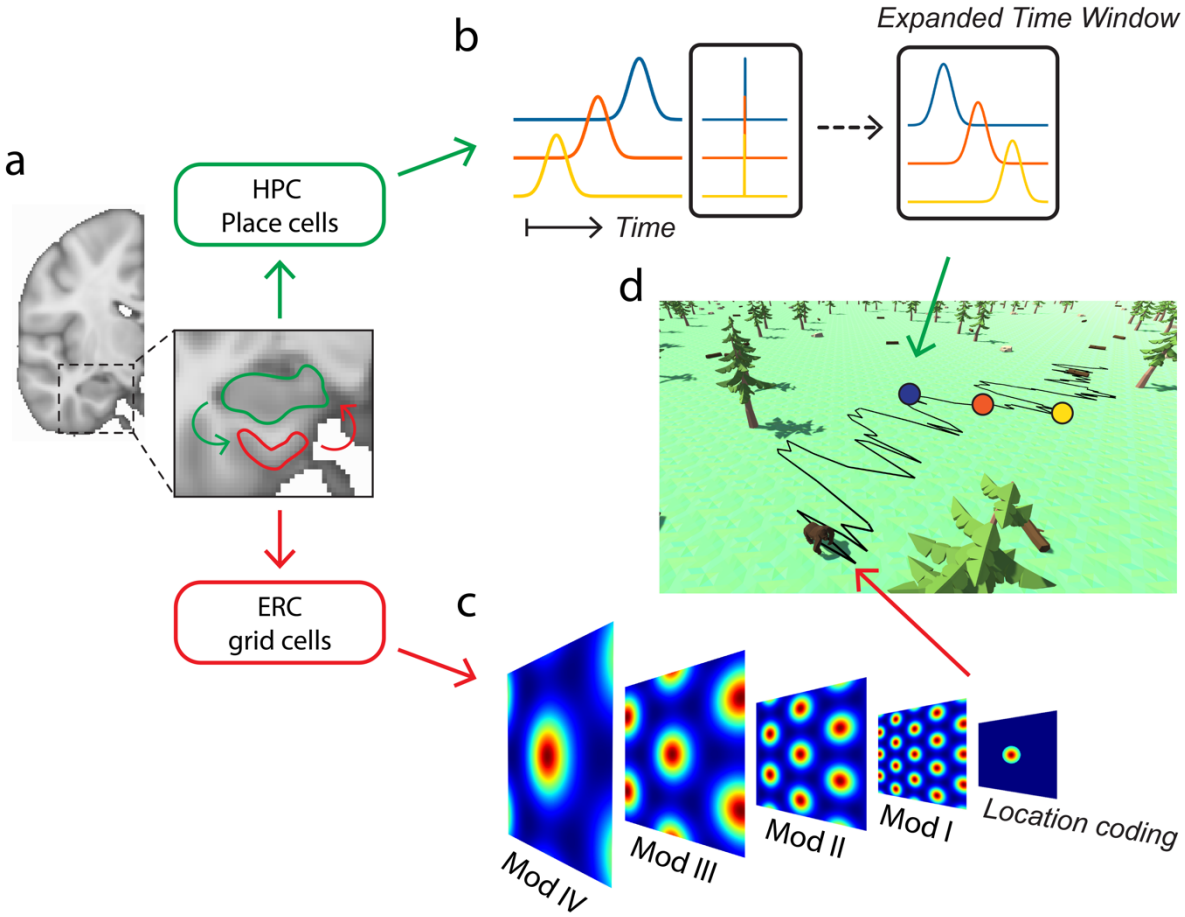

Figure 1. Anatomical and functional schematic of the HPC-ERC system. (a)-(c) Reverse replay of place cells in the Hippocampus (HPC) that represents past experience is proposed to assist in the construction of a cognitive map organized by grid cells in the Entorhinal cortex (ERC). In this system, a single location in the map is encoded by a unique population of grid cells across multiple scales. (d) The experience replay and the activation of grid cells coincide when a virtual gorilla explores a novel environment. The colored circles on the trajectory shown in (d) represent the place cells shown in (b), the sequence of locations, organized by the place cells, is replayed in time-compressed manner at a pause location pointed by a green arrow.

Results

The CAN model was utilized to simulate the formation of the hexagonal pattern of grid cells (Burak and Fiete, 2009; Couey et al., 2013; Shipston-Sharman et al., 2016; Khona & Fiete, 2022). In this model, the attractor, which is regulated by the excitation-inhibition weight function, corresponds to the integrated head direction signals from 0° to 360°, radiating from a given location. The attractors interact within a two-dimensional lattice network, thus generating excitation-inhibition dynamics (see model parameters in Table 1 and details in Methods). The scales of the attractors (i.e., grid scales), are determined by the spatial frequency of the excitation-inhibition weight function and comprise four predefined scales to accommodate high-resolution spatial coding (Fig.1c & Fig.S4, scale [i.e., Mod] I, II, III, and IV; see Methods for details; Fiete et al., 2008; Stemmler et al., 2015; Bush et al., 2015).

In the study, a virtual gorilla was designated to mimic an animal navigating an open environment, while the model simulated the navigation using walking direction as an input (Fig.1d). To examine the effect of experience replay on hexagonal pattern formation, we first built a model with reverse replay (Fig.2a-c). In the model, experience replay (i.e., the location sequence) was directionally reversed relative to the actual experience and applied to the model at each pause location, which is consistent with the consolidation of past experience (Foster & Wilson, 2006; Ambrose et al., 2016; Gillespie et al., 2021). Each experience was constituted by either 5, 10, or 15 footsteps, representing the length of past experience. Adapting to the rapid grid pattern formation observed in studies on visual space coding (Staudigl et al., 2018; Julian et al., 2018), we constrained the gorilla's movement to three directions (i.e., 70°, 115°, or 160°) during navigation. After conducting 15 independent simulations, the spatial periodicity of grid cells, indexed by Grid-score, was assessed.

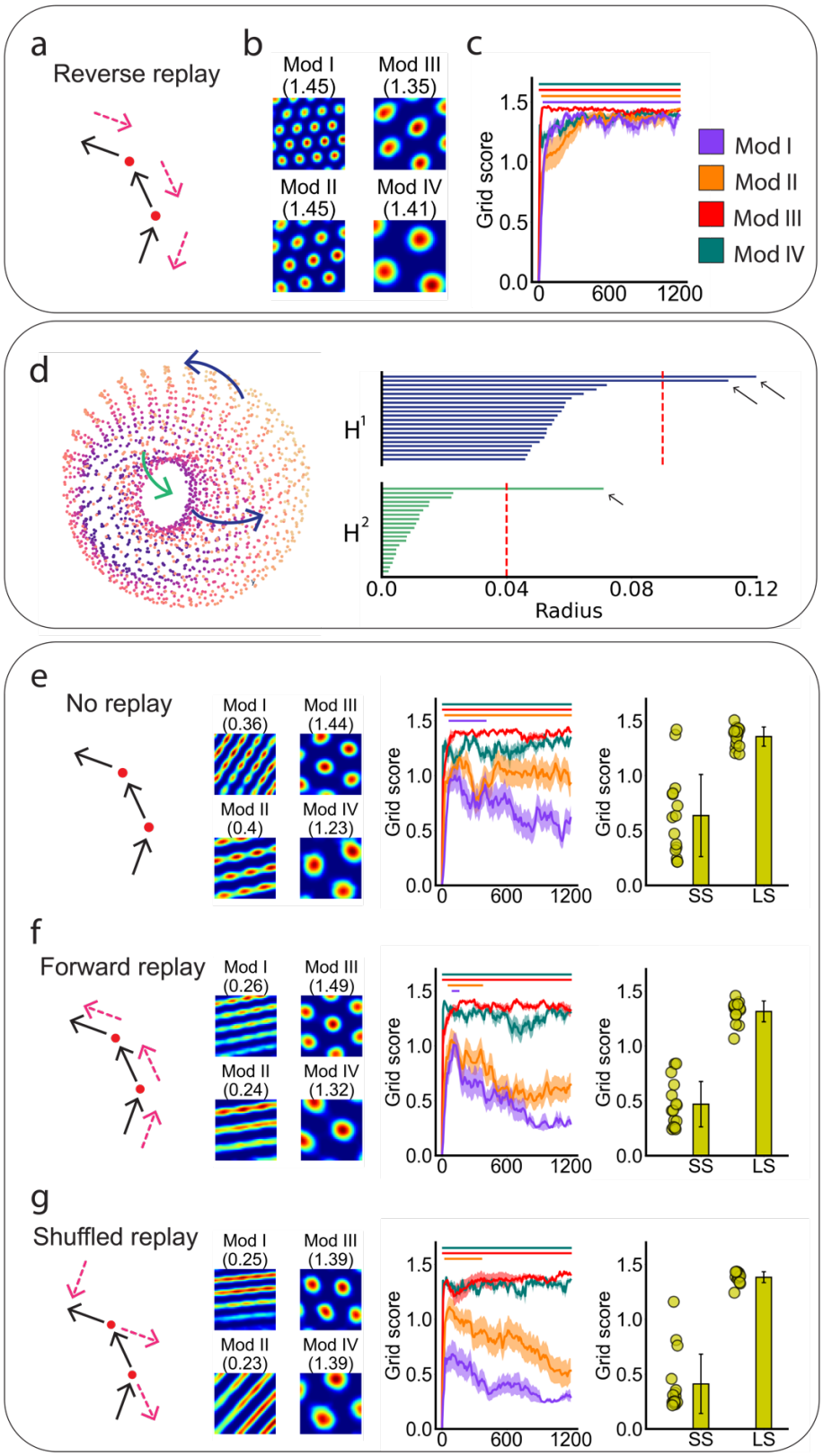
a
Reverse replay
b
Mod I (1.45)
Mod III (1.35)
Mod II (1.45)
Mod IV (1.41)
c
Grid score
Mod I
Mod II
Mod III
Mod IV
d
H1
H2
Radius
e
No replay
Mod I (0.36)
Mod III (1.44)
Mod II (0.4)
Mod IV (1.23)
SS
LS
f
Forward replay
Mod I (0.26)
Mod III (1.49)
Mod II (0.24)
Mod IV (1.32)
g
Shuffled replay
Mod I (0.25)
Mod III (1.39)
Mod II (0.23)
Mod IV (1.39)

101

Figure 2. Effect of experience replay on the formation of multi-scale grid cells. (a) Schematic representation of animal movement trajectories. Black arrows denote the direction of animal movement, and red arrows denote the direction of replay. (b) An example of multi-scale grid cells generated by the CAN model. Values in the brackets indicate Grid-score. (c) The development of the hexagonal pattern. Grid-score, averaged across grid cell populations at different scales and across 15 independent simulations, increased as a function of the number of model iterations. Solid lines above the developmental trajectories indicate that Grid-score reached significance ($p < 0.05$, initial threshold, $p < 0.05$; corrected for multiple comparisons), and error bars denote standard error. (d) A torus-like structure, derived from dimensionality reduction from the population activity of 484 grid cells of Mod IV. Barcodes with the 20 longest lifetimes from persistent cohomology analysis are shown for the 1D hole (H^1, blue) and 2D hole (H^2, green). The red dashed line indicates the threshold of significance corrected for multiple comparison (radius = 0.083 / 0.024 for H^1 / H^2, respectively). (e)-(g) Models simulated by no replay (e), forward replay (f), and shuffled-experience replay (g), respectively. The bar charts show the overall Grid-score across four scales, and a dot denotes the averaged Grid-score from one simulation. Note that all models underwent same number of iterations. SS (Mod I & II) and LS (Mod III and IV) denotes small- and large-scale, respectively.

Regular hexagonal patterns emerged for all grid scales, accompanied by a rapid increase in spatial periodicity at the beginning of simulations (Fig.2b & c & Fig.S2a, mean Grid-score of Mod I / Mod II / Mod III / IV = 1.39 / 1.44 / 1.43 / 1.39, respectively; $p<0.05$, initial threshold, $p < 0.05$; corrected for multiple comparisons). To validate the spatial periodicity of grid cells, the topological structure of population activity from 1936 grid cells were examined (Fig.2d & Fig.S3; i.e., 484 grid cells for each scale, see Method for details). Consistent with Gardner et al. (2022), we observed a toroidal structure, as indicated by the significant lifetimes of barcodes for two one-dimensional holes (the blue arrows, representing the inner and outer hole of the torus) and one two-dimensional hole (the green arrow, indicating the cavity within the torus). Those results confirmed that, with the application of reverse replay, multi-scale hexagonal patterns were successfully formed in the CAN model, despite constrained environmental exploration.

To examine the necessity of reverse replay, three control simulations were performed. First, we examined the effect of replay using a no-replay simulation where only the actual experience was applied to the model. Interestingly, deficits in grid periodicity were revealed particularly for grid Mod I & II (Fig.2e & Fig.S2a, mean Grid-score of Mod I / Mod II = 0.49 / 0.77), where grid periodicity showed a transient increase from the beginning, followed by a sharp decrease to yield a stripe pattern (Yang et al., 2004). In contrast, grid periodicity was observed for large-scale (LS, Mod III & IV, mean Grid-score of Mod I / Mod II = 1.42 / 1.29; $p<0.05$, initial threshold, $p < 0.05$; corrected for multiple comparisons). Second, we examined the direction-dependency of replay by applying forward replay, which is hypothesized for predicting future (Carr et al., 2011; Pfeiffer, 2020), wherein the location sequence was sent to the model preceding the actual experience. This manipulation resulted in a similar pattern with the no-replay simulation (Fig.2f & Fig.S2a, mean Grid-score of Mod I / Mod II = 0.29 / 0.64; mean Grid-score of Mod III & IV = 1.32 / 1.30; $p < 0.05$, initial threshold, $p < 0.05$; corrected for multiple comparisons). Third, we examined the role of the relational structure of reverse replay by shuffling the order of experiences. Again, scrambling the spatial-temporal structure of reverse replay significantly reduced the Grid-score in grid Mod I & Mod II (Fig.2g & Fig.S2a, mean Grid-score of Mod I / Mod II 0.29 / 0.53) and had little effect on grid Mod III & Mode IV (mean Grid-score of Mod III / Mod IV = 1.40 / 1.36; $p < 0.05$, initial threshold, $p < 0.05$; corrected for multiple comparisons).

Taken together, these findings suggest that reverse replay, which offers a sequential structure opposite to actual experience, is significantly more effective for the formation of

hexagonal patterns in small scales than in large scales. No effect was observed with no replay, forward replay, or shuffled-experience replay (fig.2e-g right; Mod I & II versus Mod III & IV: $t(14) = 7.02 / 13.89 / 13.28$ for no replay, forward replay, and shuffled-experience replay, respectively, $p < 0.001$, two-sided), suggesting the necessity of reversed replay in constructing a high-resolution cognitive map.

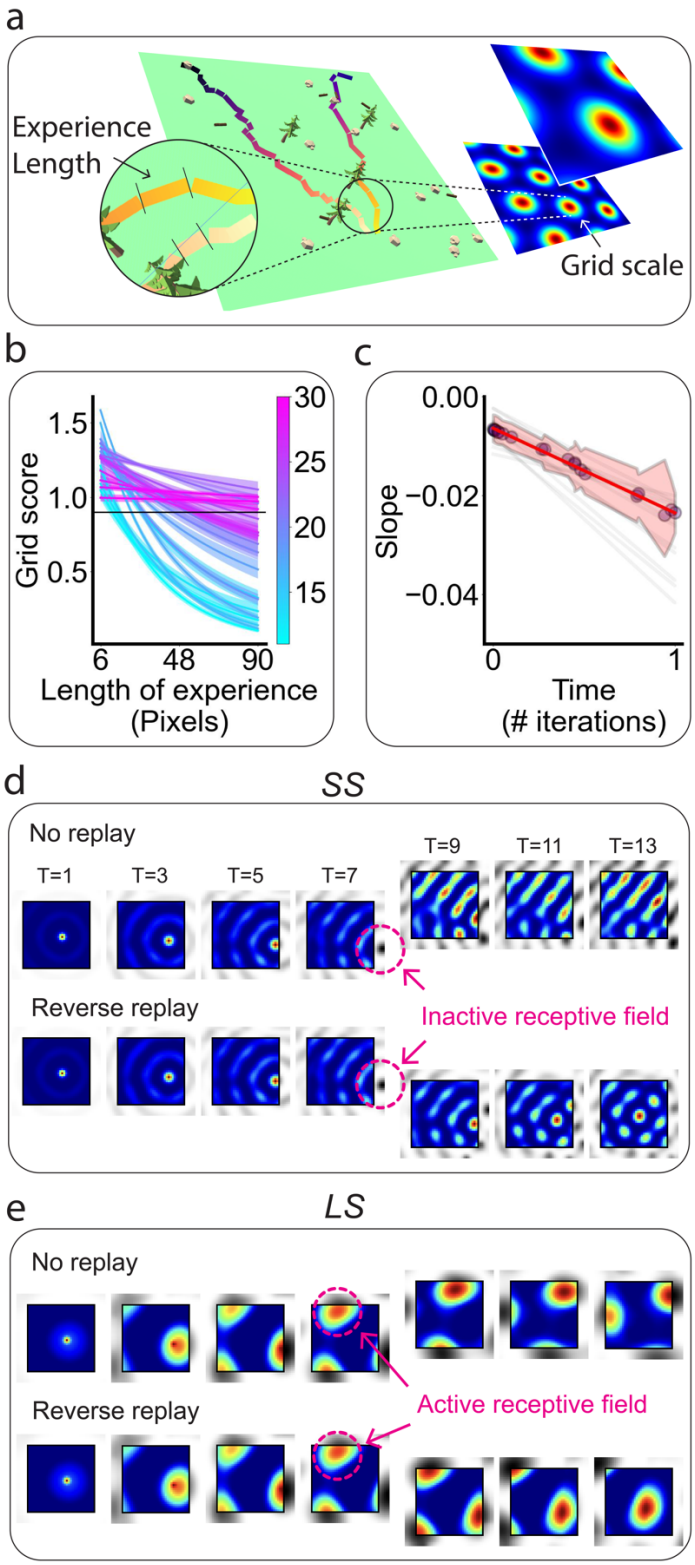

Figure 3. Mechanism of reverse replay on hexagonal pattern formation. (a) Schematic diagram that illustrates the manipulation of experience length and grid scale in the simulation. (b) Grid-score changes, represented as a function of experience length and grid scale, are fitted by an exponential decay function (R^2=0.62, P<.0.001). (c) The interaction

of experience length and grid scale, indexed by the slope (i.e., decay rate), predicted the temporal dynamics of hexagonal pattern formation during iterations (R^2=99.3%, P<0.001). (d) & (e) Two representative cases that illustrate how reverse replay influences grid periodicity, particularly in the case of small-scale (SS). In the SS case (d), after the rapid formation of periodicity during T1-5, the immediate recall (i.e., reverse replay) maintained the excitation of the already-constructed receptive field by propagating it back to the space during T9-13. This process effectively prevented the disruption of a grid-like pattern to a stripe-like pattern. In contrast, in the LS case (e), there was an earlier formation (T3-5) of grid periodicity than the SS case (T7-9). Specifically, the newly constructed receptive fields in T7 played a role in excitation-inhibition dynamics, which prevented the disruption of spatial structure even though the original receptive field propagated out of the space.

Why was the formation of LS hexagonal pattern apparently unaffected by experience replay? To address this question, we explored the mechanism underlying the role of reverse replay in the formation of hexagonal patterns. Previous studies suggest two fundamental characteristics of hippocampal replay. One is the characteristic of memory consolidation in encoding past experience (Ambrose et al., 2016; Pfeiffer, 2020), which selectively strengthens valuable memories via credit assignment (Foster & Wilson 2006; Mattar and Daw, 2018; Liu et al., 2021). The other is the anatomy of multi-scale representations of place cells along the anteroposterior axis of HPC (Brunec et al., 2018； Harland et al., 2021), which simultaneously provides both coarse and fine-grained coding to facilitate the accurate capturing of environmental complexity through replay (Wu & Foster, 2014). Based on the two characteristics, we asked how relational structures (i.e., consolidated memory), indexed by Grid-score, changed as a function of the length of immediate past experience (LPE), indexed by the number of footsteps in a single episode (Fig.3a, Left), and the wavelengths of the grid pattern (WGP) for nonlocal learning (Foster & Wilson 2006; Mattar and Daw, 2018; Liu et al., 2021), indexed by grid scales (Fig.3a, Right). Accordingly, we simulated models with 12 pairs of LPE and WGP parameters (see Table.S1, and Methods for details), respectively, and examined how Grid-score changed as a function of LPE and WGP.

As expected, we observed a significant main effect of LPE ($F(1,576) = 499.8$, $P < 0.001$) and WGP ($F(1,576) = 556.6$, $P < 0.001$) (Fig.S6), suggesting better spatial periodicity with more immediate recall (i.e., shorter LPE) and with larger scales of grid cells (i.e., larger WGP), respectively. Interestingly, the decay rate in spatial periodicity along LPE, indexed by decay slope k (see Methods for details), varied as a function of WGP. That is, smaller scales of grid cells were associated with a faster decay rate, where decay slope k strongly correlated with grid cell scales ($R^2 = 0.62$, $P < 0.001$). This observation was further confirmed by a significant modulation effect of WGP when the replay was applied as opposed to no replay (replay: $F(1,576) = 117.8$, $p < 0.001$; no replay: $F(1,576) = 0.84$, $p = 0.36$). Critically, the slope k, determined under the interaction of LPE and WGP, predicted the time needed to form a grid pattern with a satisfactory Grid-score (Fig.3c & Fig.S7; R^2=99.3%, $P<0.001$). For example, the formation time of grid cells of a smaller scale associated with more immediate recall (i.e., a smaller k) was equivalent to the formation time of grid cells of a larger scale associated with less immediate recall.

This observation thus provides a potential explanation for the role of reverse replay in maintaining relational structures through grid cells of varying scales. For example, when a small-

scale grid cell traverses through space, a grid-like pattern forms quickly (T = 5, Fig.3d, left), showing an initial increase in Grid-score at the development stage (Fig.2). However, because of the small receptive field of this grid cell, the active receptive field, which preferentially represents the self-location formed by the CAN model (Fig.S4), easily propagates out of the space (T = 7, Fig.3d, middle). In the absence of replay, the grid-like pattern disintegrates into a stripe-like pattern (T = 11, Fig.3d, top right). In contrast, immediate recall (i.e., reverse replay) enables the receptive field to propagate back into the space, allowing the maintenance and further development of the grid-like pattern (T = 13, Fig.3d, top bottom). On the other hand, a large-scale grid cell not only possesses a larger receptive field that remains active for a longer duration (T = 7, Fig.3e) but also forms a grid-like pattern more quickly (Fig.3c & Fig.S7); therefore, a regular grid pattern is formed before the receptive field becomes inactive. Accordingly, reverse replay is no longer needed for pattern maintenance. Therefore, the effect of reverse replay on grid periodicity depends on the interplay of multiple factors, such as environmental characteristics (e.g., the size and structure of the space), biological properties (e.g., grid scales/WGP, time constant τ of CAN, and length of past experience/LPE), and actual navigation behaviors (e.g., movement direction).

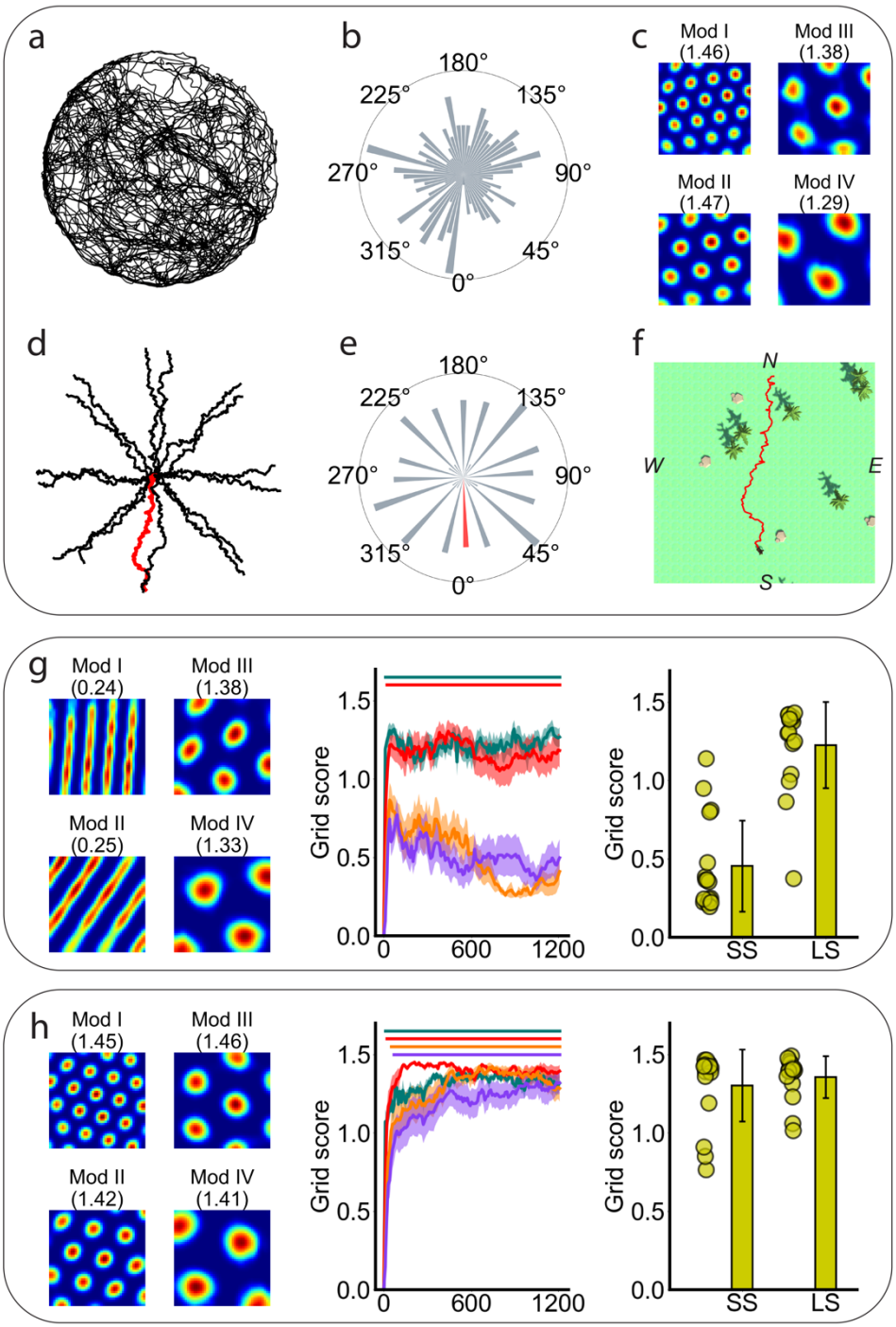

Figure 4. Effect of the amount of exploration on the formation of multi-scale grid cells. (a) Animal trajectories obtained from open-source data (Hafting et al., 2005), (b) A polar plot denoting the distribution of movement directions, (c) An example of the multi-scale grid cells generated by the CAN model without the application of experience replay; Grid-score is shown in bracket. (d)-(f) Simulated trajectories with movement directions uniformly distributed across 0°-360° as indicated by the Polar plot. Each trajectory was governed by a global direction with noise bounded by -90° - 90°. For example, the trajectory with a global direction towards South, highlighted in red, was associated to the

movement directions of 270° ± 90°. (g)-(h) Models simulated with no replay and reverse replay, respectively; the line and bar charts showed the overall Grid-score across four scales performed from 16 independent simulations (d-e). Note that the same number of iterations were applied to all models.

To clearly demonstrate this point, we predict that even small-scale grid cells do not necessitate reverse replay to form regular hexagonal patterns if their receptive fields remain active through continuous change in the direction of movement, thus confining the receptive field within the space. This is precisely what animals do. An analysis of mouse movement traces (Fig.4a, Hafting et al., 2005) showed that the movement directions were uniformly distributed from 0° to 360° ($p = 0.23$, Rayleigh test, Fig.4b). Furthermore, when we applied the same trace to the virtual gorilla, regular periodicity was observed for all grid scales without the need for replay (Fig.4c, Grid-score= 1.46/1.47/1.38/1.29 for Mod I / II / III / IV, respectively. $p < 0.05$, initial threshold, $p < 0.05$; corrected for multiple comparisons).

To further examine the necessity of this strategy, we designed trajectory traces, each of which aimed towards a global direction with random noise of direction applied at each local location (Fig.4d-f and Fig.S8, $p < 0.001$, Rayleigh test; see Methods for details). In this scenario, the receptive field likely propagates out of the space before the hexagonal pattern forms reliably. Indeed, without replay, we observed a stripe pattern in small-scale grid cells (Fig.4g & Fig.S2b, mean Grid-score of Mod I / Mod II = 0.49 / 0.41, respectively), which had a significantly lower Grid-score than that of large-scale grid cells ($t(15) = 7.47$, $p<0.001$, two-sided). As expected, the irregularity in periodicity was eliminated with reverse replay (Fig.4h & Fig.S2b, mean Grid-score= 1.32 / 1.28 / 1.39 / 1.32, for Mod I / II / III / IV, respectively. $p < 0.05$, initial threshold, $p < 0.05$; corrected for multiple comparisons), significantly more regular than that without replay (Fig.4h, $t(15) = 8.85$, $p<0.001$, two-sided). Considering the habit of animals to randomly change direction while navigating novel environments, reverse replay seems not necessary. However, it becomes critical, especially for small-scale grid cells, when animals need to rapidly form hexagonal patterns of grid cells with limited environmental exploration.

Discussion

This study utilized the CAN model to examine the role of experience replay in facilitating the hexagonal pattern formation of grid cells. We found that reverse replay, as opposed to no replay, forward replay, or shuffled-experience replay, significantly enhanced grid periodicity. Specifically, experience replay was particularly effective in enhancing the spatial periodicity of small-scale grid cells, thus assisting in the construction high-resolution cognitive map. Further analyses revealed that the relationship between experience replay and hexagonal pattern formation was modulated by the interplay between the spatial scales of grid cells and the length of past experience, which ensured that the active receptive field was not disrupted by wave propagation by balancing between the size of grid scale and the duration of past experience. In summary, our results revealed a causative relationship between experience replay and hexagonal pattern formation from a computational perspective. This revelation may provide insights into how reverse reactivations of hippocampal place cell construct abstract knowledge structures by facilitating the hexagonal pattern formation of Entorhinal grid cells (Suh et al., 2013; Wu and Foster, 2014; Liu et al., 2019; Nour et al., 2021; Hafting et al., 2005; McNaughton et al., 2006; Behrens et al., 2018).

One distinct advantage of computational modelling is to allow for careful and intentional manipulation of all parameters. In this study, we utilized the CAN model to simulate the excitation-inhibition dynamics of grid cells (Burak and Fiete, 2009; Couey et al., 2013; Shipston-Sharman et al., 2016; Kang and Balasubramanian, 2019; Khona & Fiete, 2022) and revealed two novel findings. First, under circumstances of limited environment exploration, reverse replay is necessary to form hexagonal patterns of small-scale grid cells, highlighting the potential of reverse replay to quickly and flexibly form hexagonal patterns without the need for extensive environmental exploration. This finding may help explain previous findings of grid periodicity in one-dimensional linear virtual track (Yoon et al., 2016) and circular track (Jacob et al., 2019), as well as during rapid visual mapping (Staudigl et al., 2018; Julian et al., 2018). In these irregular environments and task-dependent demands, traditional long-term exploration strategies may be less effective; in contrast, experience replay can provide a rapid and efficient mechanism to adapt to these situations, enabling quick establishment of spatial representations under various constraints.

Second, by systematically manipulating WGP (large versus small scales), LPE (long versus short experience length), and tasks (free versus limited explorations), we revealed that the effect

of reverse replay on grid periodicity is modulated by interactions of various factors, more complex than originally assumed derived from empirical studies. However, the underlying mechanism remains the same, as the function of reverse replay is to preserve the formed pattern by initiating reverse replay before the active receptive field propagates out of space because of wave propagation. Therefore, reverse replay is particularly important for small-scale grid cells because the formation of small-scale hexagonal patterns demands more time and is therefore more susceptible to pattern disruption, suggested by the reaction-diffusion model where Turing instability varied as a function of spatial frequency in pattern formation (Yang et al., 2004).

The distinct dynamics of small and large grid scales dovetail nicely with the multi-scale representation observed in the anterior (ventral) and posterior (dorsal) HPC (Strange et al., 2014; Schiller et al., 2015). The anterior HPC encodes coarse-grained experiences represented by large-scale receptive fields, while the posterior HPC encodes fine-grained experiences with small-scale receptive fields. Specifically, the posterior HPC, the site commonly selected for recording neuronal replay (Bendor & Wilson, 2012; Carr et al., 2012; Gillespie et al., 2021), might be specifically involved in the hexagonal pattern formation of small-scale grid cells with the presence of experience replay. This conjecture is supported by the occurrence of hippocampal sharp wave ripples, which facilitate experience replay and are typically characterized by transient high-frequency oscillations for precise location coding (Buzsáki, 2015; Ambrose et al., 2016).

This study has a number of limitations. First, we primarily relied on computational modelling based heavily on the dynamic properties of the CAN model; therefore, the findings may not fully capture the hexagonal pattern formation of grid cells and the interplay of Hippocampal place cells and Entorhinal grid cells. Future studies are needed to test other models on grid cells (Dordek et al., 2016; Monsalve-Mercado & Leibold, 2017; Whittington et al., 2020; Gao et al., 2021; Schaeffer et al., 2022) and conduct empirical experiments on these testable hypotheses. Second, we focused solely on the function of reverse replay on the hexagonal pattern formation of grid cells. Previous studies, however, demonstrate that neuronal replay also plays critical role in memory consolidation and retrieval (Carr et al., 2011), learning (Momennejad, 2020), and emotional processing (Rihm & Rasch, 2015), for example. Thus, a more comprehensive integration of the functionality of replay is needed possibly by exploring their relations in future experiments (Kurth-Nelson et al., 2023). Finally, our CAN simulations for entorhinal space representation were driven by predefined pseudorandom movements, rather than self-organized

path integration guided by hippocampal goal representation (Ormond & O'Keefe, 2022). To address this limitation, future studies need to develop a unified HPC-ERC system that not only simulates the HPC-to-ERC pathway for generating entorhinal metrics using reverse replay but also includes the ERC-to-HPC pathway to generate hippocampal forward replay with direction integrated for self-location updating (Wu and Foster, 2014; Pfeiffer, 2020). The integration of the HPC and ERC in a single model may help unveil principles of the grid-place cell system for navigation in mental spaces, including the visual space (Nau et al., 2018), object space (Constantinescu., 2016), and reward space (Sosa and Giocomo, 2021).

Data availability

Raw data reported in the present study are available from the corresponding author upon reasonable request.

Code availability

Python and .NET code for grid cell simulation and virtual navigation are available at https://github.com/ZHANGneuro/Hippocampal-replay-facilitates-the-formation-of-entorhinal-grid-cells. Scripts for the analysis reported in the present study are available from the corresponding author upon reasonable request.

Conflict of interest

None declared.

Author Contributions

B.Z. and J.L. conceived the study; B.Z. built the computational model and performed the analysis; L.M. provided valuable advice and assistance; B.Z. and J.L. wrote the paper.

Acknowledgments

We thank Dr. Yunzhe Liu for providing valuable comments on the manuscript. This work was supported by the National Key R&D Program of China (2020AAA0105200), China Postdoctoral Science Foundation (2022M710470), Beijing Municipal Science & Technology Commission & Administrative Commission of Zhongguancun Science Park (Z221100002722012), Tsinghua University Guoqiang Institute (2020GQG1016), and Beijing Academy of Artificial Intelligence (BAAI).

Supplemental Material

"Experience replay facilitates the formation of the hexagonal pattern of grid cells"

Bo Zhang, Lei Ma, and Jia Liu

Methods

Task and design

Spatial navigations were simulated in a 3D squared open environment created by Unity (Unity Technologies, San Francisco). For each simulation, a borderless novel environment was created with trees, tree trunks, and stones randomly placed on a flat grassy ground. A virtual Gorilla acts as the animal and was arranged to perform either limited or extended explorations in the environment, during which Gorilla's navigational experiences were passively driven by pre-defined allocentric directions. Specifically, for the limited exploration, we constrained the number of directions to three, each 45° apart (70°,115°, and 160° with 0° pointing towards East). Those directions were randomly assigned to each footstep during simulation. For the extended exploration, we arranged for the Gorilla to move in hundreds of directions. These were either derived from open-source data (Hafting et al., 2005; https://www.ntnu.edu/kavli/research/grid-cell-data), or predefined following one of eight global directions, each 45° apart (0°, 45°, 90°, 135°, 180°, 225°, 270°, and 315°). In the latter case, the Gorilla's direction at each footstep was determined by a global direction plus an additional noise randomly assigned from a range of -90° to 90°. This resulted in, for example, a range of walking directions from 0° to 180° for the simulation with a global direction of 90° (Fig.3d).

Continuous attractor network

To examine the impact of experience-replay on grid periodicity, we utilized CAN model, programmed by Torch (Version 1.13, Python version 3.9), for simulating the hexagonal pattern of grid cells. Meanwhile, the model accepted Gorilla's walking directions as input with the experience intentionally manipulated by applying either No, Reverse, Forward, or Shuffled experience replay. Specifically, in the no-replay, the model accepted a list of Gorilla's walking directions in each episode. In the forward replay, a list of walking directions identical with the actual experience was sent to the model in advance. In the reverse replay, the walking directions were reversed and were sent to the model following the actual experience. In Shuffled replay, which aimed to examine the necessity of sequential structure of past experience, we applied the reversed walking directions to the model with the directions shuffled within the episode after actual experience. To ensure the stability of model inference, each manipulation of experience replay was independently simulated 15 times for the limited exploration (three directions) and 16 times for

extended exploration (twice for each of eight global directions), then group-level tests were conducted. The length of episode was defined by the number of footsteps with size of each footstep of 3 pixels (approximately 1 virtual meter in virtual environment). In both limited and extended experiment, a single episode was randomly assigned with either 5-, 10-, or 15- footsteps. A pause location, mimicking animal's decision point, was placed in the temporal gap of two consecutive episodes (Fig.2e-g). To measure the impact of experience-length (LPE) on Grid-score (how Grid-score changes as a function of LPE), a total of 29 LPE, ranged from 2 to 30 footsteps with a step of 1, was additionally prepared. To examine the impact of LPE on Grid-score dynamics (how fast Grid-score reaches the significance threshold), we measured the slope $-\frac{1}{k}$ of the exponential decay function $ae^{(\frac{-LPE}{k})}$, which was first linearized via log transformation and was subsequently fitted by the curve_fit function of scipy package (version 1.9.3). In all the simulations, the maximum of footsteps across episodes was constrained by 1200. The number of footsteps in the open-source dataset (Hafting et al., 2005) was down-sampled to 1200 data points.

To simulate grid cell population by CAN. A two-dimension matrix of membrane voltage ξ, defined with the size of 45-by-45 pixel with each location representing a single neuron, was created. In each footstep, under certain walking direction v and step size, the membrane voltages of grid cells are updated by the differential equation (equation 1). Specifically, the excitation or inhibition signal, used to update the membrane voltage ξ_i of neuron i, is determined by the firing rates of all potential neuron j that connect with neuron i and the corresponding connection weight W_{ij} between the neuron i and neuron j. τ and ε denotes time constant and gaussian noise, respectively.

$$\tau \frac{d\xi_i}{dt} = -\xi_i + \sum_j W_{ij} f_j + v_i + \varepsilon \tag{1}$$

The firing rate f_j of neuron j, derived from the membrane voltage ξ_j via a nonlinear transfer function (equation 2), will be inhibited to 0 if its membrane voltage is not exceeding a threshold η, otherwise the f_j of neuron j is determined by the square root of membrane voltage ξ_j, leading to a connection to neuron i via W_{ij}.

$$f_j = \begin{cases} \sqrt{\xi_j} & \xi_j > \eta \\ 0 & \zeta_j \leqslant \eta \end{cases} \tag{2}$$

The weight W, a two-dimensional matrix where the value in the matrix represents the connection strength of neurons (equation 3), was predefined by averaging all potentially possible head directions ranged from 0° to 360° with each represented by a planar wave, indicating the spatial representation of head directions on two-dimensional space (see Fig.S4 & Table.S1 for details). Specifically, a planar wave in certain direction θ is formalized by $\cos(\omega(\nu_x X + \nu_y Y))$, where ν_x and ν_y, derived by $\cos(\theta)$ and $\sin(\theta)$, determine the direction of activity gradient $\nu_x X + \nu_y Y$ in physical space.

$$W_{ij} = \sum_{\theta=0}^{359} \alpha \cos(\omega(\upsilon_x X + \upsilon_y Y)) \tag{3}$$

The spatial frequency ω in equation 3 is derived from grid scales σ (equation 4), each of which represents the Euclidean distance between the peaks of two adjacent grid fields. For example, the grid scale $\sigma = 10$ (i.e., 10 pixels, approximately 3.3 virtual meters) demonstrates a lower spatial resolution in compared to the grid scale $\sigma = 5$. To examine the impact of grid scales on the formation of hexagonal patterns of grid cell, a total of 20 grid scales, ranged from 11 to 30 pixels, were prepared (see Table 1 for details).

$$\omega = 2pi/\sigma \tag{4}$$

<u>Edge effect of grid cell simulation</u>

Edge effect is an intrinsic issue in grid cell simulation, which denotes the distortion of hexagonal patterns because the grid codes near the edge of space receive less connections via recurrent weights relative to that far away from the edge (Fuhs and Touretzky, 2006). Samsonovich and McNaughton (1997) hypothesized the twisted representation of grid cells, which deals with the issue of edge effect by wrapping the mental space to toroidal structure so that the neurons close to the edges can be connected to each other, reflecting the property of spatial periodicity. Inspired by this idea, we employed interpolation to overcome the issue of edge effects (Fig.S5). Particularly, grid orientation and phase are computed in advance so that when and where the grid fields come

in the space from the opposite edge could be predicted after they reach the edge and propagate out of space. Specifically, we derive the grid orientation by computing the autocorrelation maps of hexagonal pattern (Hafting et al., 2005). Next, the neural activity for each target pixel is interpolated using trigonometric function, which computes the grid phase based on grid scale and one out of six coordinates that located on the three main axis of hexagonal pattern inside the space . Finally, one coordinate was randomly selected and the activity strength was interpolated into the target pixel after excluding the coordinates outside of space. With this procedure, the issue of edge effect is solved by the spatial periodicity characterized by grid orientation and phase.

<u>Validation of grid periodicity</u>

The spatial periodicity of gird cell, as indicated by Grid-score, was computed by following the procedure reported previously (Sargolini et al., 2006; Barry & Burgess, 2017). Specifically, for each neuron generated by the models, the spatial autocorrelation map was estimated by equation 5, where $\lambda(x, y)$ denote the activity strength at location (x, y), while τ_x and τ_y denote the spatial shifts of the firing pattern from the neuron. With the rotation of autocorrelation map by 30°, 60°, 90°, 120°, and 150°, Grid-scorewas computed as the difference between the lowest correlation of 60° and 120° and the highest correlations of 30°, 90° and 150°.

$$r(\tau_x,\tau_y) = \frac{n\sum\lambda(x,y)\lambda(x-\tau_x,y-\tau_y)-\sum\lambda(x,y)\lambda(x-\tau_x,y-\tau_y)}{\sqrt{n\sum\lambda(x,y)^2(\sum\lambda(x,y))^2}\sqrt{n\sum\lambda(x-\tau_x,y-\tau_y)^2(\sum\lambda(x-\tau_x,y-\tau_y))^2}} \quad (5)$$

For the regularity of grid cell population, we examined the toroidal structure of population activity of grid cells using persistent homology (Ghrist, 2008), which was performed by the package Ripser++ (Version 1.1.2) for GPU acceleration (Zhang et al., 2020; Bauer, 2021). The principle behind persistent homology is to identify the toroidal characteristics from the global topological feature constituted by point-clouds (the firing maps of grid cell) in 3D Euclidean space. Specifically, we followed the outlines published previously (Gardner et al., 2022). At each grid scale, principal component analysis was performed on the population activity of grid cells, then the first six principal components were further dimension-reduced by uniform manifold approximation into 3D projection. In the 3D space, the data points were Z transformed and were replaced with simplicial complexes. Upon increasing the radius of simplicial complexes, the complexes are gradually connected and form certain global structure. To examine the emergence

of toroidal structure, the life spans (the barcodes) of two 1D holes (the inner and outer hole of torus) and one 2D hole (the cavity in the interior of torus) were tracked throughout the duration of holes from it appear to disappear. Assuming that the life time of a given hole were long enough, the hole would be considered to be contained robustly by the global structure of connected complexes.

Statistics

To quantifying the periodicity of firing patterns generated by CAN, the significance threshold was accessed by field-shuffling permutation (Fig.S9; Krupic et al., 2012). The threshold was derived from the models with reverse-replay applied, which produced the most regular hexagonal patterns across grid scales. Specifically, the long-range spatial structure (global structures of firing field) of given firing pattern was disrupted by shuffling the firing fields 100 times with the local structure (single firing field) preserved. The uncorrected threshold was then determined by the 95th percentile of the shuffling distribution. The significant threshold corrected for multiple comparison was further determined by the 95th percentile of the uncorrected-threshold distribution computed from grid cell population. Similar procedure was used for persistent cohomology analysis, in which the initial uncorrected threshold and the corrected threshold was indicated by the 99th and 95th percentile of the barcode distribution from single and population neurons, respectively. The significance thresholds for the toroidal structure of 1D (H1) and 2D hole (H2) were then averaged across grid scales. The effect of experience-length and grid scales on grid periodicity/grid dynamics were quantified using ANOVA/Pearson correlation, respectively. The difference in grid periodicity between small- and large-scales was examined using two sample t-test. All the t-tests used in the present study were two-tailed.

Figure S1. Grid cell population generated by CAN model using animal trajectories acquired from open-source data (Hafting et al., 2005). For each scale, 24 grid cell samples were shown as example and were sorted by phase along the horizontal and vertical axis.

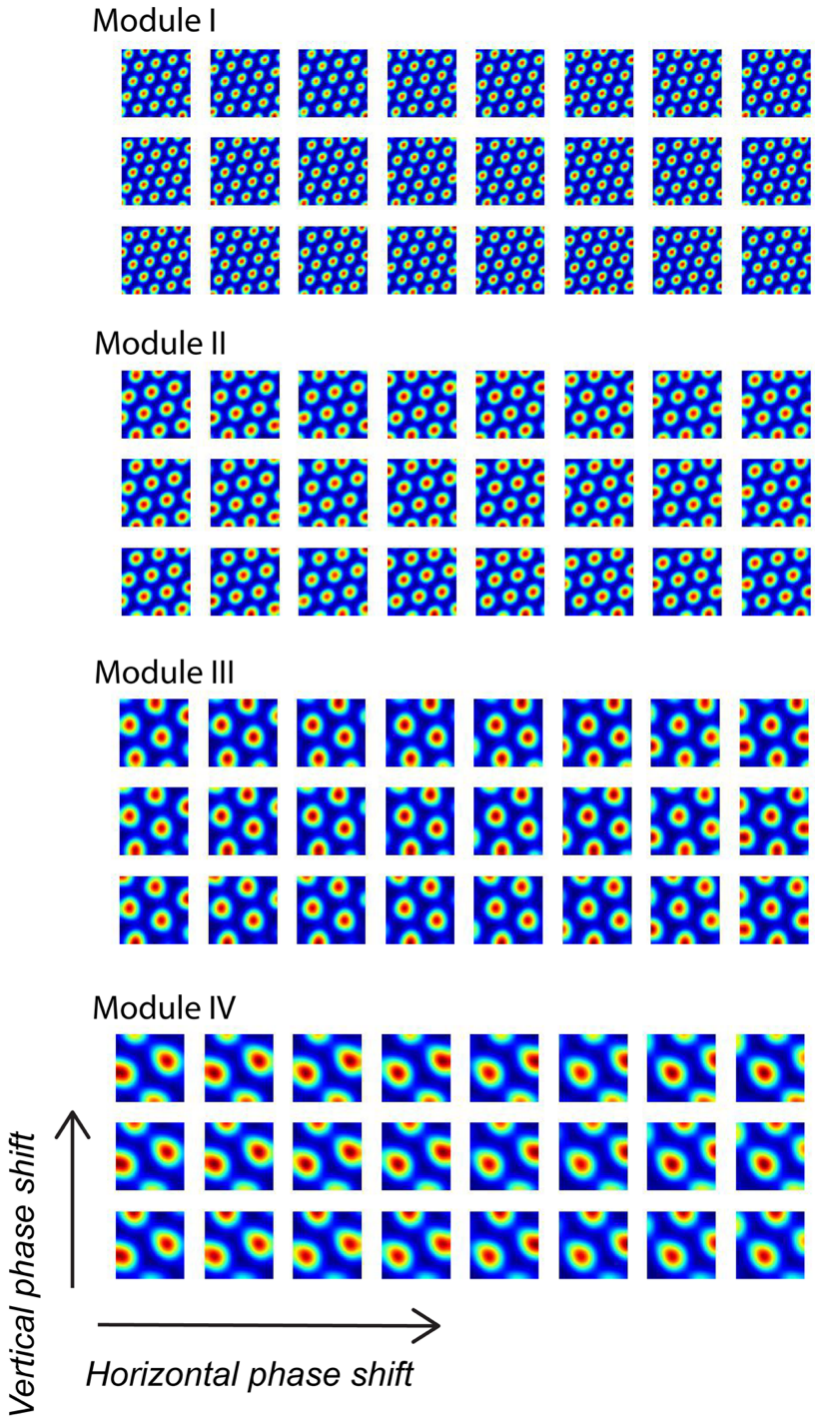

Figure S2. Extended comparison of Grid-score among the replay manipulations in corresponding to Fig.2 and 4. 15 and 16 independent simulations were performed for (a) and (b), respectively.

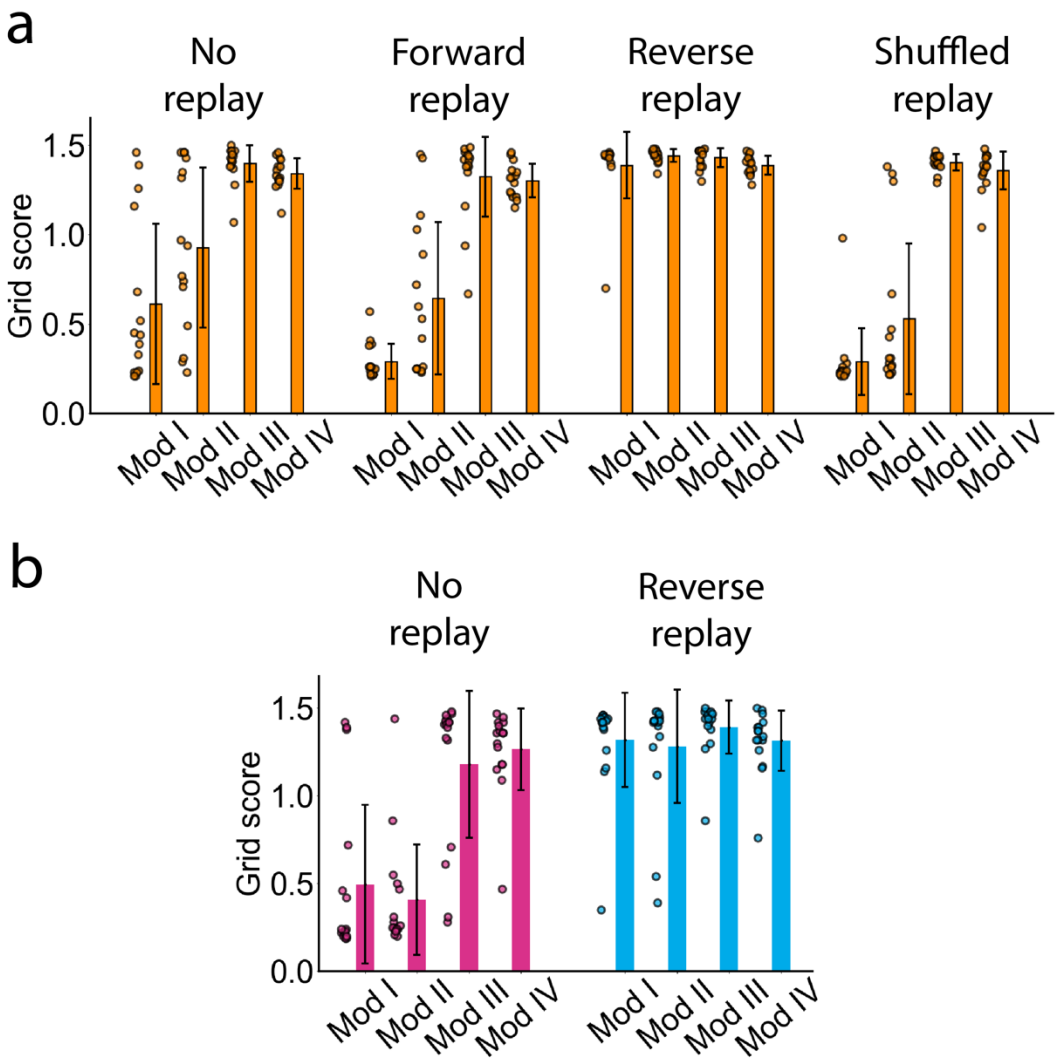

Figure S3. Persistent cohomology analysis on the population activity (484 grid cells) of each grid scale, which were derived from the model with reverse replay applied shown in Fig.2. The barcodes with 20 longest lifetimes were shown for the 1D hole (H1, blue) and 2D hole (H2, green), red dash lines indicate the threshold of significance corrected for multiple comparison.

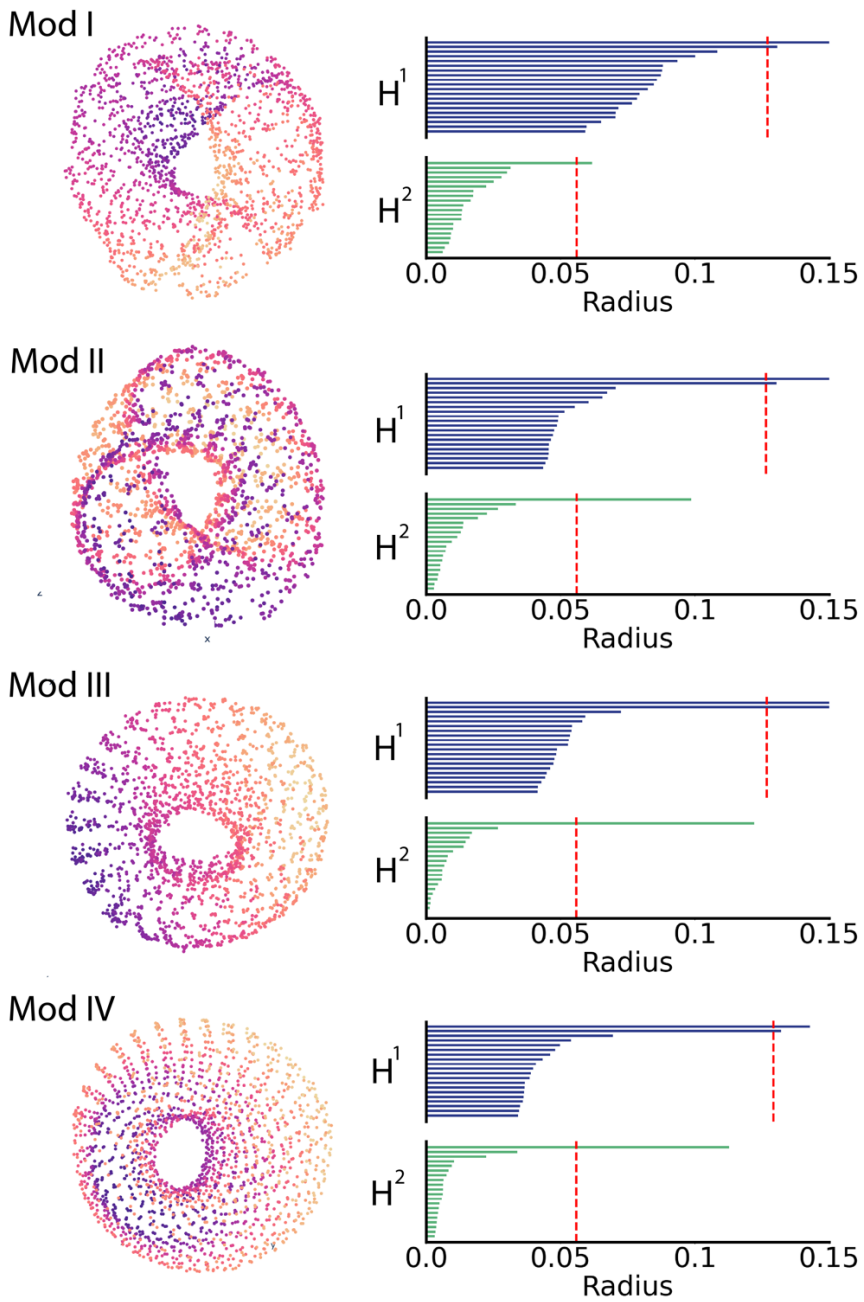

Figure S4. Illustration of the formation of grid cell using CAN model. a) Example of the weight matrix (grid Mod I), which represents the conjunctive head directions of 0° - 360° for a given allocentric location. Each head direction was embedded by a planar wave that represents the unique direction across locations on the two-dimensional space. b) the formation of hexagonal pattern with model iterations (T), regular grid periodicity could be seen by T = 60.

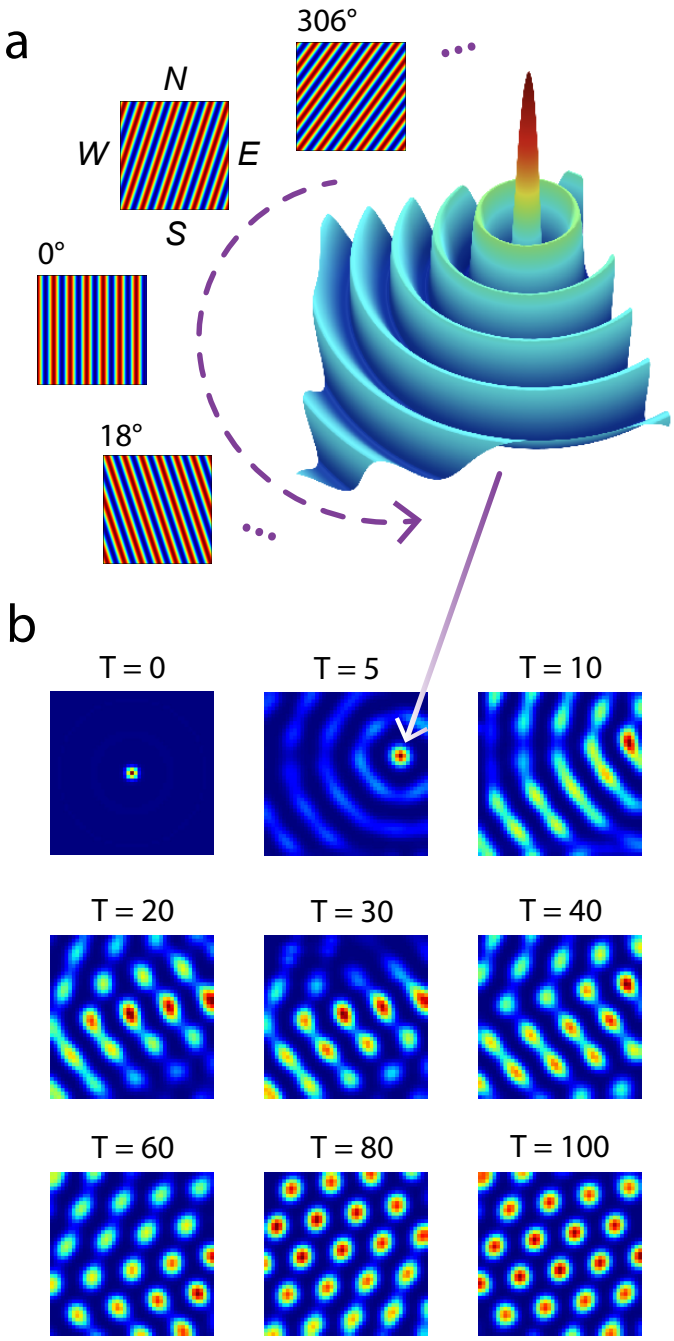

Figure S5. Simulation of grid cell population using interpolation. a) the original hexagonal pattern without phase shifting, b) grid orientation was computed from the autocorrelation map of the original hexagonal pattern, c) an example of interpolation procedure. Aligning with the twisted representation of hexagonal pattern, each pixel in the blank area (colored by white) induced by the phase shift towards North was interpolated from one out of six adjacent locations computed by grid orientation and phase using trigonometric function. d) the hexagonal pattern with phase shifted relative to the original pattern shown in (a).

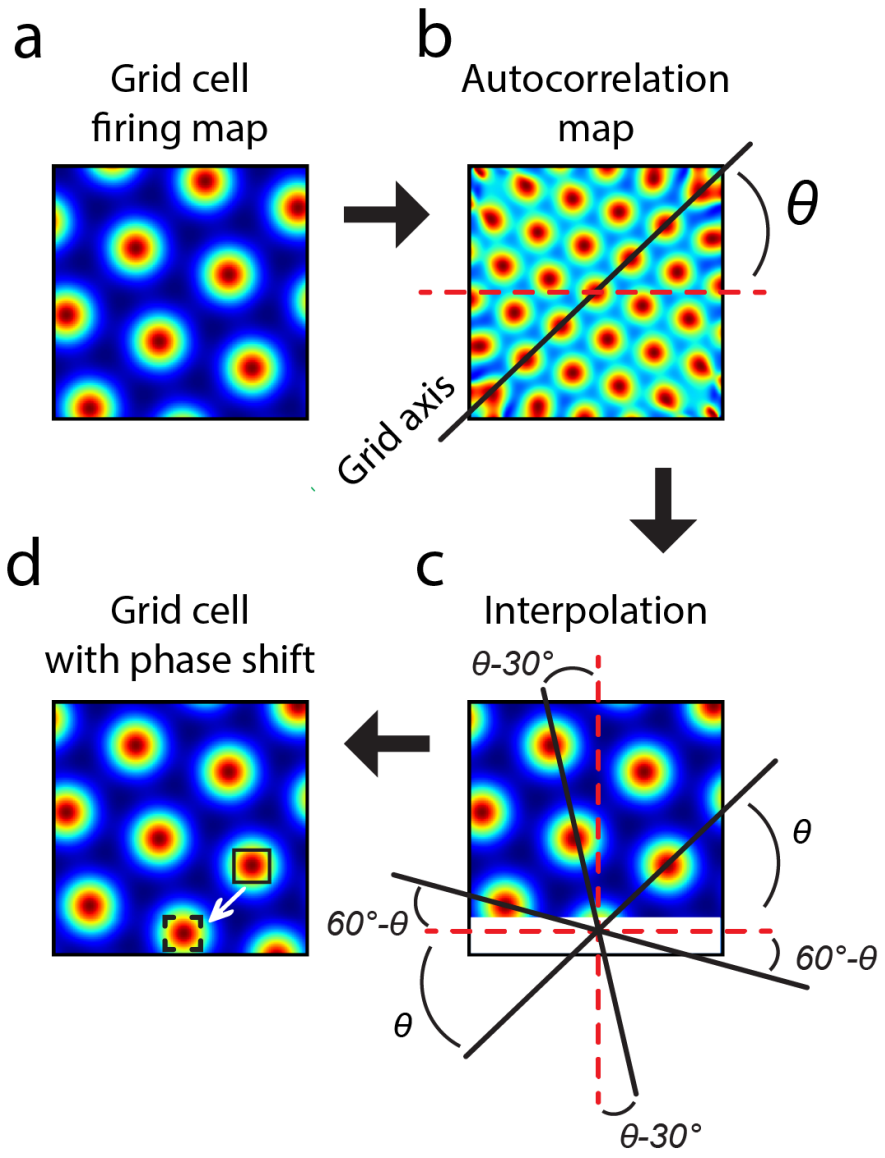

Figure S6. Effect of experience-length and grid scale on grid periodicity. Black/Red line represents the models with no-/reverse-replay applied, respectively. Dashed line indicates the significance threshold of Grid-score. Error bar denotes the standard error of 12 independent simulations.

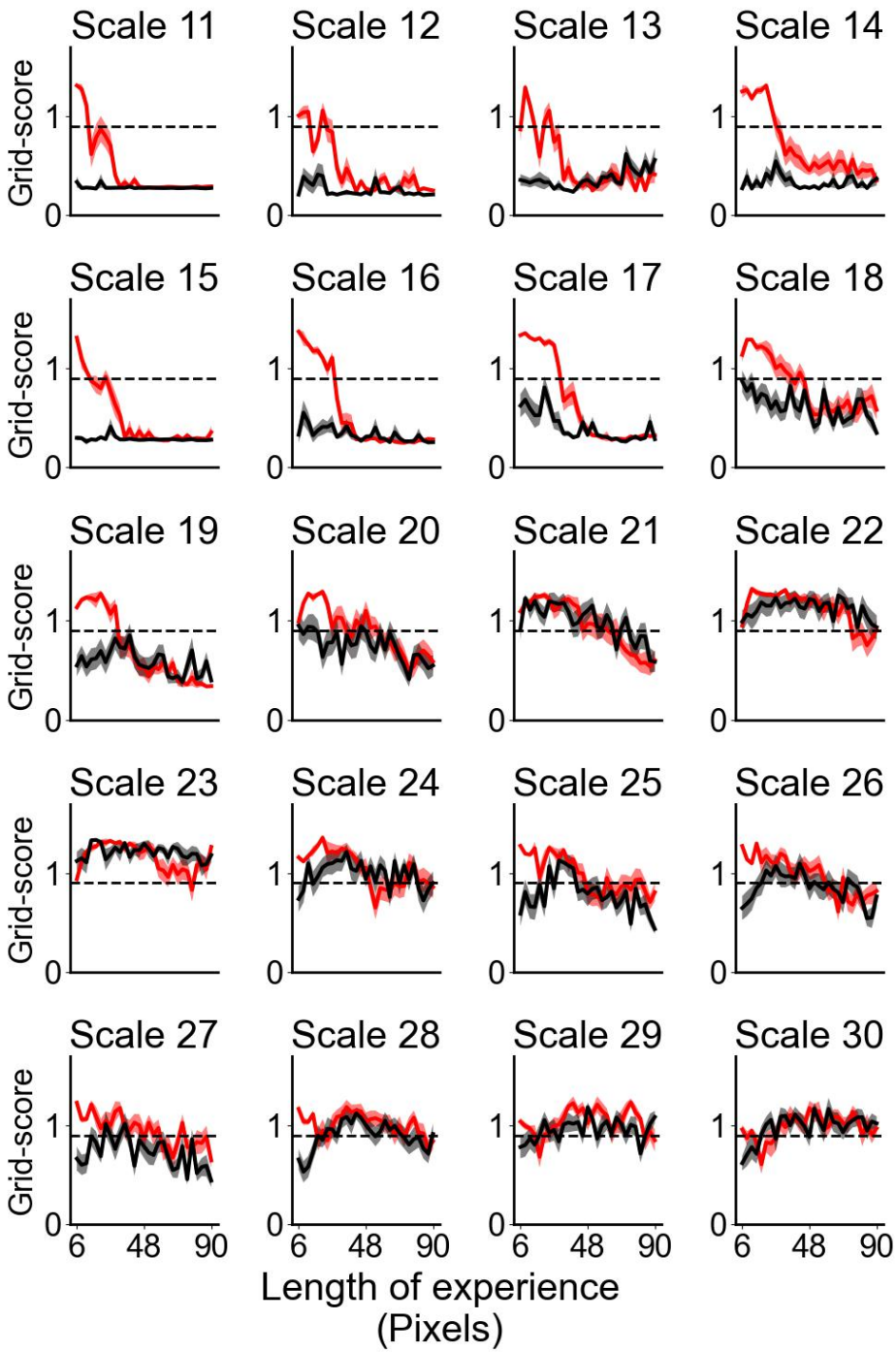

Figure S7. Grid-score changes as a function of iteration. The grid periodicity of large-scale increases faster than the one of small-scale. Red line indicates the iteration where Grid-score reaches the significance threshold. Error bar denotes the standard error of 12 independent simulations.

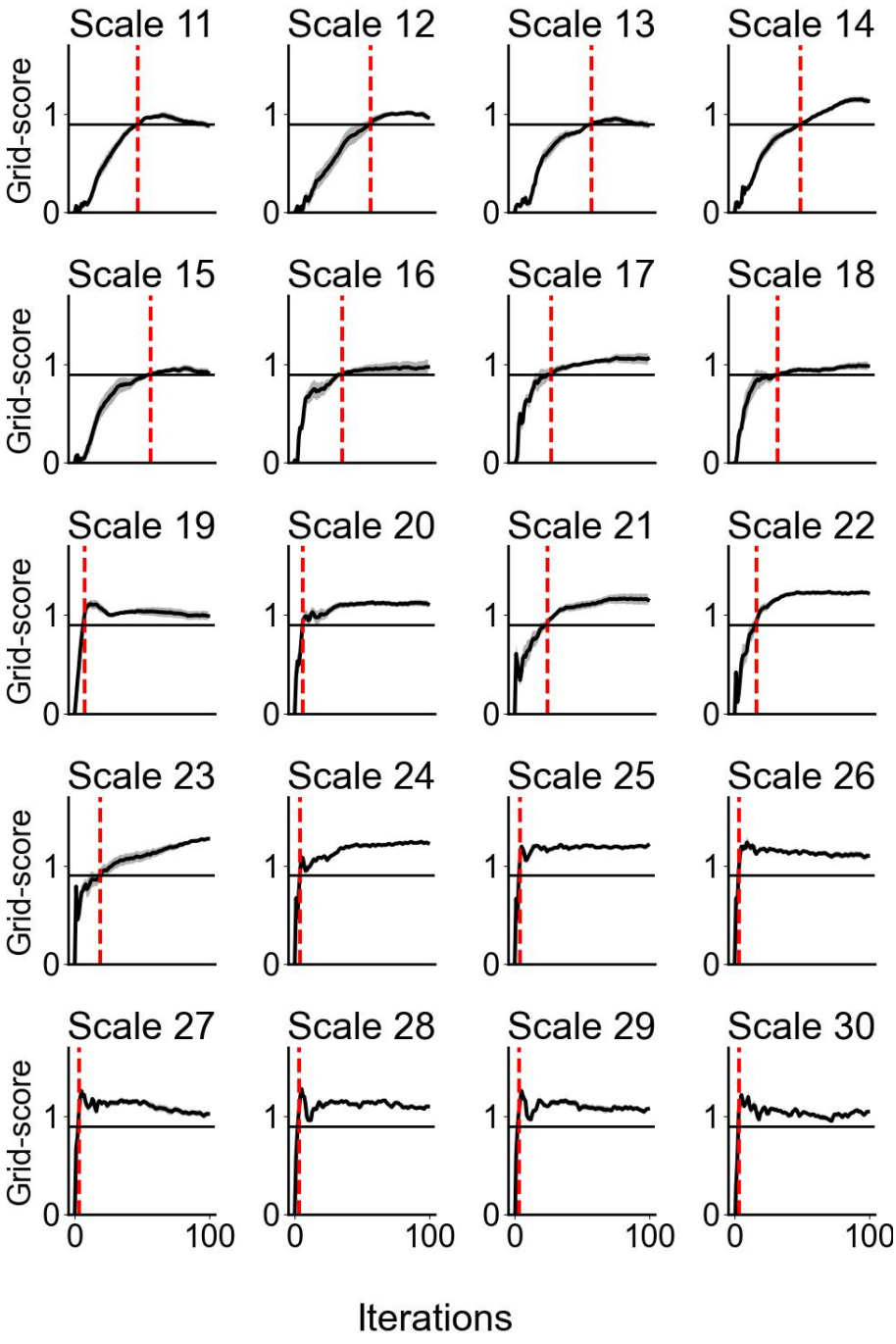

Figure S8. Sixteen independently simulated virtual navigations for each of no-replay and reverse-replay model. Each virtual navigation was dominated by a unique global direction with the noise ranged from -90° to 90° for each footstep. Left column, the distribution of movement directions, black solid line indicates the mean of directions, Right column, Gorilla trajectories during virtual navigation.

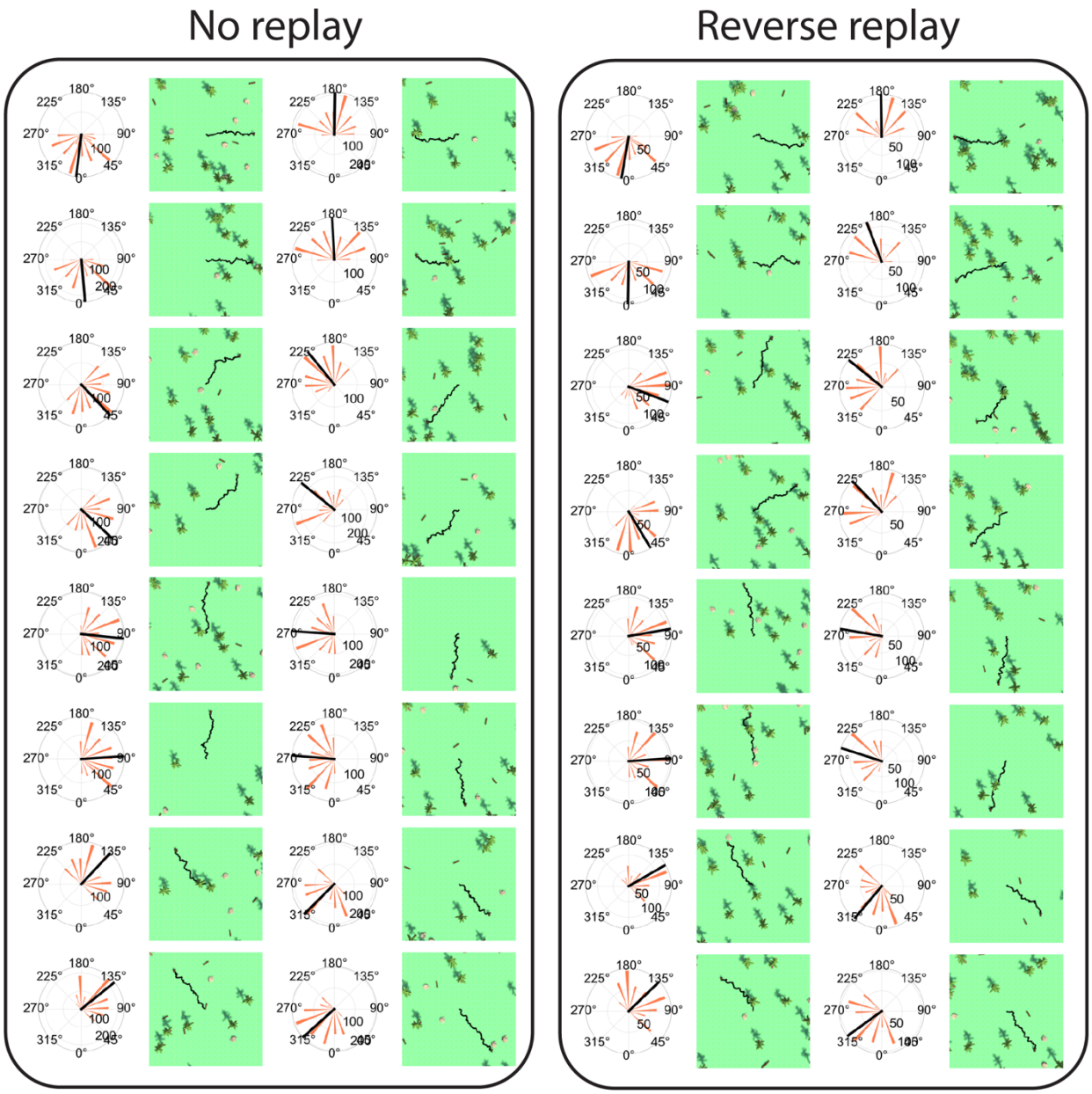

Figure S9. Procedure of field-shuffling permutation. 1) an example of hexagonal pattern, 2) extracting the peaks of the firing field, 3) identifying the local structure of hexagonal pattern, outlined by polygons using Voronoi polygons, 4-5) the firing field that was randomly re-positioned during field-shuffling, (6) the shuffled hexagonal pattern of grid cell, (7) the Grid-score distribution derived from 100 field-shuffling, the black dash line represents the initial (uncorrected) threshold at the 99th percentile of Grid-score distribution, (8) the uncorrected Grid-score distribution derived from grid cell population, black dash line represents the corrected threshold for multiple comparison at the 95th percentile of the distribution.

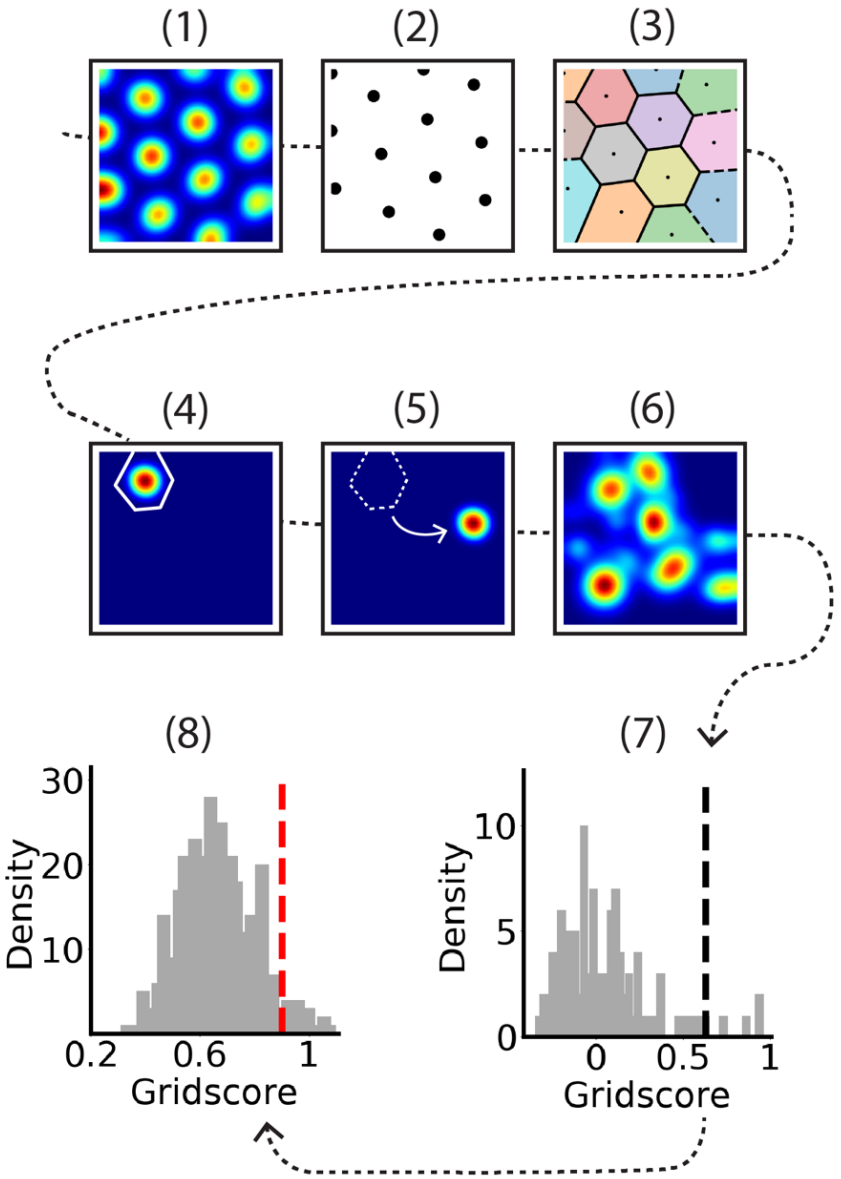

Table S1. Model parameters.

Parameter	Variable	Value
Membrane voltage threshold	η	0
Time constant	τ	10
Weight matrix	W	
Positive peak		0.003
Negative peak		-0.001
Mean		0
Amplitude of planar wave	α	0.333
Grid scales	$\vec{\sigma}$	11-30 pixels (20 samples)
Space size	N	45 pixels

Reference

Ambrose, R. E., Pfeiffer, B. E., & Foster, D. J. (2016). Reverse replay of hippocampal place cells is uniquely modulated by changing reward. Neuron, 91(5), 1124-1136.

Barry, C., & Burgess, N. (2017). To be a Grid Cell: Shuffling procedures for determining "Grid-score". BioRxiv, 230250.

Bauer, U. (2021). Ripser: efficient computation of Vietoris–Rips persistence barcodes. Journal of Applied and Computational Topology, 5(3), 391-423.

Bendor, D., & Wilson, M. A. (2012). Biasing the content of hippocampal replay during sleep. Nature neuroscience, 15(10), 1439-1444.

Burak, Y., & Fiete, I. R. (2009). Accurate path integration in continuous attractor network models of grid cells. PLoS computational biology, 5(2), e1000291.

Barry, C., Ginzberg, L. L., O'Keefe, J., & Burgess, N. (2012). Grid cell firing patterns signal environmental novelty by expansion. Proceedings of the National Academy of Sciences, 109(43), 17687-17692.

Behrens, T. E., Muller, T. H., Whittington, J. C., Mark, S., Baram, A. B., Stachenfeld, K. L., & Kurth-Nelson, Z. (2018). What is a cognitive map? Organizing knowledge for flexible behavior. Neuron, 100(2), 490-509.

Burgess, N., Maguire, E. A., & O'Keefe, J. (2002). The human hippocampus and spatial and episodic memory. Neuron, 35(4), 625-641.

Bonnevie, T., Dunn, B., Fyhn, M., Hafting, T., Derdikman, D., Kubie, J. L., ... & Moser, M. B. (2013). Grid cells require excitatory drive from the hippocampus. Nature neuroscience, 16(3), 309-317.

Buzsáki, G. (2015). Hippocampal sharp wave-ripple: A cognitive biomarker for episodic memory and planning. Hippocampus, 25(10), 1073-1188.

Bush, D., Barry, C., Manson, D., & Burgess, N. (2015). Using grid cells for navigation. Neuron, 87(3), 507-520.

Brunec, I. K., Bellana, B., Ozubko, J. D., Man, V., Robin, J., Liu, Z. X., ... & Moscovitch, M. (2018). Multiple scales of representation along the hippocampal anteroposterior axis in humans. Current biology, 28(13), 2129-2135.

Couey, J. J., Witoelar, A., Zhang, S. J., Zheng, K., Ye, J., Dunn, B., ... & Witter, M. P. (2013). Recurrent inhibitory circuitry as a mechanism for grid formation. Nature neuroscience, 16(3), 318-324.

Carr, M. F., Jadhav, S. P., & Frank, L. M. (2011). Hippocampal replay in the awake state: a potential substrate for memory consolidation and retrieval. Nature neuroscience, 14(2), 147-153.

Carr, M. F., Karlsson, M. P., & Frank, L. M. (2012). Transient slow gamma synchrony underlies hippocampal memory replay. Neuron, 75(4), 700-713.

Constantinescu, A. O., O'Reilly, J. X., & Behrens, T. E. (2016). Organizing conceptual knowledge in humans with a gridlike code. Science, 352(6292), 1464-1468.

Dordek, Y., Soudry, D., Meir, R., & Derdikman, D. (2016). Extracting grid cell characteristics from place cell inputs using non-negative principal component analysis. Elife, 5, e10094.

Foster, D. J., & Wilson, M. A. (2006). Reverse replay of behavioural sequences in hippocampal place cells during the awake state. Nature, 440(7084), 680-683.

Fiete, I. R., Burak, Y., & Brookings, T. (2008). What grid cells convey about rat location. Journal of Neuroscience, 28(27), 6858-6871.

Fuhs, M. C., & Touretzky, D. S. (2006). A spin glass model of path integration in rat medial entorhinal cortex. Journal of Neuroscience, 26(16), 4266-4276.

Gardner, R. J., Hermansen, E., Pachitariu, M., Burak, Y., Baas, N. A., Dunn, B. A., ... & Moser, E. I. (2022). Toroidal topology of population activity in grid cells. Nature, 602(7895), 123-128.

Gillespie, A. K., Maya, D. A. A., Denovellis, E. L., Liu, D. F., Kastner, D. B., Coulter, M. E., ... & Frank, L. M. (2021). Hippocampal replay reflects specific past experiences rather than a plan for subsequent choice. Neuron, 109(19), 3149-3163.

Ghrist, R. (2008). Barcodes: the persistent topology of data. Bulletin of the American Mathematical Society, 45(1), 61-75.

Gao, R., Xie, J., Wei, X. X., Zhu, S. C., & Wu, Y. N. (2021). On path integration of grid cells: group representation and isotropic scaling. Advances in Neural Information Processing Systems, 34, 28623-28635.

Hafting, T., Fyhn, M., Molden, S., Moser, M. B., & Moser, E. I. (2005). Microstructure of a spatial map in the entorhinal cortex. Nature, 436(7052), 801-806.

Hales, J. B., Schlesiger, M. I., Leutgeb, J. K., Squire, L. R., Leutgeb, S., & Clark, R. E. (2014). Medial entorhinal cortex lesions only partially disrupt hippocampal place cells and hippocampus-dependent place memory. Cell reports, 9(3), 893-901.

Harland, B., Contreras, M., Souder, M., & Fellous, J. M. (2021). Dorsal CA1 hippocampal place cells form a multi-scale representation of megaspace. *Current Biology*, *31*(10), 2178-2190.

Jacob, P. Y., Capitano, F., Poucet, B., Save, E., & Sargolini, F. (2019). Path integration maintains spatial periodicity of grid cell firing in a 1D circular track. Nature Communications, 10(1), 1-13.

Julian, J. B., Keinath, A. T., Frazzetta, G., & Epstein, R. A. (2018). Human entorhinal cortex represents visual space using a boundary-anchored grid. Nature neuroscience, 21(2), 191-194.

Khona, M., & Fiete, I. R. (2022). Attractor and integrator networks in the brain. Nature Reviews Neuroscience, 1-23.

Kang, L., & Balasubramanian, V. (2019). A geometric attractor mechanism for self-organization of entorhinal grid modules. Elife, 8.

Krupic, J., Burgess, N., & O'Keefe, J. (2012). Neural representations of location composed of spatially periodic bands. Science, 337(6096), 853-857.

Kurth-Nelson, Z., Behrens, T., Wayne, G., Miller, K., Luettgau, L., Dolan, R., ... & Schwartenbeck, P. (2023). Replay and compositional computation. Neuron.

Liu, Y., Dolan, R. J., Kurth-Nelson, Z., & Behrens, T. E. (2019). Human replay spontaneously reorganizes experience. Cell, 178(3), 640-652.

Liu, Y., Mattar, M. G., Behrens, T. E., Daw, N. D., & Dolan, R. J. (2021). Experience replay is associated with efficient nonlocal learning. Science, 372(6544), eabf1357.

Moser, E. I., Moser, M. B., & McNaughton, B. L. (2017). Spatial representation in the hippocampal formation: a history. Nature neuroscience, 20(11), 1448-1464.

McNaughton, B. L., Battaglia, F. P., Jensen, O., Moser, E. I., & Moser, M. B. (2006). Path integration and the neural basis of the 'cognitive map'. Nature Reviews Neuroscience, 7(8), 663-678.

Monsalve-Mercado, M. M., & Leibold, C. (2017). Hippocampal spike-timing correlations lead to hexagonal grid fields. Physical review letters, 119(3), 038101.

Mattar, M. G., & Daw, N. D. (2018). Prioritized memory access explains planning and hippocampal replay. Nature neuroscience, 21(11), 1609-1617.

Momennejad, I. (2020). Learning structures: predictive representations, replay, and generalization. Current Opinion in Behavioral Sciences, 32, 155-166.

Nau, M., Schröder, T. N., Bellmund, J. L., & Doeller, C. F. (2018). Hexadirectional coding of visual space in human entorhinal cortex. Nature neuroscience, 21(2), 188-190.

Nour, M. M., Liu, Y., Arumuham, A., Kurth-Nelson, Z., & Dolan, R. J. (2021). Impaired neural replay of inferred relationships in schizophrenia. Cell, 184(16), 4315-4328.

Ormond, J., & O'Keefe, J. (2022). Hippocampal place cells have goal-oriented vector fields during navigation. Nature, 607(7920), 741-746.

Pfeiffer, B. E. (2020). The content of hippocampal "replay". Hippocampus, 30(1), 6-18.

Rihm, J. S., & Rasch, B. (2015). Replay of conditioned stimuli during late REM and stage N2 sleep influences affective tone rather than emotional memory strength. Neurobiology of learning and memory, 122, 142-151.

Suh, J., Foster, D. J., Davoudi, H., Wilson, M. A., & Tonegawa, S. (2013). Impaired hippocampal ripple-associated replay in a mouse model of schizophrenia. Neuron, 80(2), 484-493.

Schiller, D., Eichenbaum, H., Buffalo, E. A., Davachi, L., Foster, D. J., Leutgeb, S., & Ranganath, C. (2015). Memory and space: towards an understanding of the cognitive map. Journal of Neuroscience, 35(41), 13904-13911.

Strange, B. A., Witter, M. P., Lein, E. S., & Moser, E. I. (2014). Functional organization of the hippocampal longitudinal axis. Nature Reviews Neuroscience, 15(10), 655-669.

Samsonovich, A., & McNaughton, B. L. (1997). Path integration and cognitive mapping in a continuous attractor neural network model. Journal of Neuroscience, 17(15), 5900-5920.

Sargolini, F., Fyhn, M., Hafting, T., McNaughton, B. L., Witter, M. P., Moser, M. B., & Moser, E. I. (2006). Conjunctive representation of position, direction, and velocity in entorhinal cortex. Science, 312(5774), 758-762.

Sosa, M., & Giocomo, L. M. (2021). Navigating for reward. Nature Reviews Neuroscience, 1-16.

Shipston-Sharman, O., Solanka, L., & Nolan, M. F. (2016). Continuous attractor network models of grid cell firing based on excitatory–inhibitory interactions. The Journal of physiology, 594(22), 6547-6557.

Schuck, N. W., & Niv, Y. (2019). Sequential replay of nonspatial task states in the human hippocampus. Science, 364(6447), eaaw5181.

Schultz, W., Dayan, P., & Montague, P. R. (1997). A neural substrate of prediction and reward. Science, 275(5306), 1593-1599.

Stemmler, M., Mathis, A., & Herz, A. V. (2015). Connecting multiple spatial scales to decode the population activity of grid cells. Science Advances, 1(11), e1500816.

Staudigl, T., Leszczynski, M., Jacobs, J., Sheth, S. A., Schroeder, C. E., Jensen, O., & Doeller, C. F. (2018). Hexadirectional modulation of high-frequency electrophysiological activity in the human anterior medial temporal lobe maps visual space. Current Biology, 28(20), 3325-3329.

Schlesiger, M. I., Cannova, C. C., Boublil, B. L., Hales, J. B., Mankin, E. A., Brandon, M. P., ... & Leutgeb, S. (2015). The medial entorhinal cortex is necessary for temporal organization of hippocampal neuronal activity. Nature neuroscience, 18(8), 1123-1132.

Schacter, D. L., Addis, D. R., & Buckner, R. L. (2007). Remembering the past to imagine the future: the prospective brain. Nature reviews neuroscience, 8(9), 657-661.

Schaeffer, R., Khona, M., & Fiete, I. (2022). No free lunch from deep learning in neuroscience: A case study through models of the entorhinal-hippocampal circuit. bioRxiv, 2022-08.

Tulving, E., & Markowitsch, H. J. (1998). Episodic and declarative memory: role of the hippocampus. Hippocampus, 8(3), 198-204.

Tolman, E. C. (1948). Cognitive maps in rats and men. Psychological review, 55(4), 189.

van Groen, T., Miettinen, P., & Kadish, I. (2003). The entorhinal cortex of the mouse: organization of the projection to the hippocampal formation. Hippocampus, 13(1), 133-149.

Vaz, A. P., Wittig Jr, J. H., Inati, S. K., & Zaghloul, K. A. (2020). Replay of cortical spiking sequences during human memory retrieval. Science, 367(6482), 1131-1134.

Wu, X., & Foster, D. J. (2014). Hippocampal replay captures the unique topological structure of a novel environment. Journal of Neuroscience, 34(19), 6459-6469.

Witter, M. P., & Amaral, D. G. (1991). Entorhinal cortex of the monkey: V. Projections to the dentate gyrus, hippocampus, and subicular complex. Journal of Comparative Neurology, 307(3), 437-459.

Whittington, J. C., Muller, T. H., Mark, S., Chen, G., Barry, C., Burgess, N., & Behrens, T. E. (2020). The Tolman-Eichenbaum machine: unifying space and relational memory through generalization in the hippocampal formation. Cell, 183(5), 1249-1263.

Yoon, K., Lewallen, S., Kinkhabwala, A. A., Tank, D. W., & Fiete, I. R. (2016). Grid cell responses in 1D environments assessed as slices through a 2D lattice. Neuron, 89(5), 1086-1099.

Yang, L., Zhabotinsky, A. M., & Epstein, I. R. (2004). Stable squares and other oscillatory Turing patterns in a reaction-diffusion model. Physical review letters, 92(19), 198303.

Zhang, S., Xiao, M., & Wang, H. (2020). GPU-accelerated computation of Vietoris-Rips persistence barcodes. arXiv preprint arXiv:2003.07989.